AIAA JOURNAL
Vol. 43, No. 11, November 2005

Fluidic Oscillation Influences on V-Shaped Bluffbody Flow

R. F. Huang* and K. T. Chang†
National Taiwan University of Science and Technology, Taipei 10672, Taiwan, Republic of China

The V-shaped fluidic oscillator is developed by inserting a target blockage with a specially designed crescent surface into the downstream cavity of a slit V gutter. Stable, self-sustained, periodic fluidic oscillations can be induced by the dynamic Coanda effect when the geometric parameters of the target blockage and the Reynolds number are properly tuned. The fluidic oscillations are directed through two slit passageways and injected into the near wake of the V-shaped fluidic oscillator like pulsing jets. The oscillation behaviors, frequency selection, streamline patterns, and turbulence properties of the unsteady flows in the near wakes of the V-shaped fluidic oscillator are studied experimentally in a wind tunnel by using the smoke-wire flow visualization technique, hot-wire anemometry, and laser Doppler velocimetry. Flowfields of the slit V gutter and the closed-tip V gutter, which are the counterparts of the V-shaped fluidic oscillator, are also measured for comparison. The Strouhal number of the fluidic oscillation based on the slit width of the presently developed oscillator can attain a value of about 0.56 at large Reynolds numbers, which is about 80 times larger than the previous results for the enhancement of heat transfer and about 60 times larger than that for the fluidic flowmeter. The fluidic oscillations act as an excitation source for the wake. The kinetic energy of the fluidic oscillations is transferred to turbulent fluctuations and therefore causes increases in the size of the recirculation bubble and the turbulence intensity in the wake of the V-shaped fluidic oscillator. The turbulence intensity in the near wake can be increased by about 7% when compared with that of the closed-tip V gutter.

Nomenclature

b_{gap}	=	gap width between V gutter wing and target blockage
d	=	slit width at vertex of V gutter
f_f	=	frequency of fluidic oscillation, Hz
f_s	=	frequency of vortex shedding in the wake, Hz
h	=	offset distance from crescent origin to virtual vertex of target blockage
L	=	span of V gutter
n	=	number of data points collected by laser Doppler velocimetry in each record
R	=	radius of crescent profile of target blockage
Re_d	=	Reynolds number based on slit width d of V gutter, $U_\infty d/\nu$
Re_W	=	Reynolds number based on cross-stream width W of V gutter, $U_\infty W/\nu$
$Sr_{d,f}$	=	Strouhal number of fluidic oscillation based on slit width d of V gutter, $f_f d/U_\infty$
$Sr_{W,f}$	=	Strouhal number of fluidic oscillation based on cross-stream width of V gutter, $f_f W/U_\infty$
$Sr_{W,s}$	=	Strouhal number of vortex shedding based on cross-stream width W of V-shaped bluffbody, $f_s W/U_\infty$
T_u	=	turbulence intensity of u velocity, u'/U_∞
T_w	=	turbulence intensity of w velocity, w'/U_∞
U	=	local instantaneous velocity measured by one-component hot-wire anemometry
U_∞	=	time-averaged freestream velocity
u	=	local instantaneous velocity in X direction measured by laser Doppler velocimetry
$\bar{u}$	=	local time-averaged velocity in X direction measured by laser Doppler velocimetry
u'	=	root mean square of fluctuating velocity in X direction, $\sqrt{[\sum_n (u-\bar{u})^2/n]}$
W	=	cross-stream width of V-shaped bluffbody
w	=	local instantaneous velocity in Z direction measured by laser Doppler velocimetry
$\bar{w}$	=	local time-averaged velocity in Z direction measured by laser Doppler velocimetry
w'	=	root mean square of fluctuating velocity in Z direction, $\sqrt{[\sum_n (w-\bar{w})^2/n]}$
X	=	streamwise coordinate originated from leading edge of V-shaped bluffbody
X_{ASP}	=	axial location of aft stagnation point of recirculation bubble behind V-shaped bluffbody
Y	=	spanwise coordinate originated from center of span of V-shaped bluffbody
Z	=	chordwise coordinate originated from leading edge of V-shaped bluffbody
ν	=	kinetic viscosity of airstream
Φ	=	power spectrum density function of fluctuation velocity

Received 23 September 2004; revision received 13 February 2005; accepted for publication 11 May 2005.

*Professor, Department of Mechanical Engineering; rfhuang@mail.ntust.edu.tw. Senior Member AIAA.
†Graduate Student, Department of Mechanical Engineering.

Introduction

A FLOW passing over a bluffbody produces complicated phenomena such as separation, recirculation, mass entrainment through the shear layers, vortex shedding in the wake, and so on.[1] Ample evidence has shown that aerodynamic characteristics of the near-wake flow behind a bluffbody have crucial influence on the transport efficiencies of momentum, mass, and energy in the wake. In general, the mixing capability, heat transfer, and combustion efficiency can be notably enhanced through strong cross-stream exchanges of the momentum and mass, which are induced primarily by unsteady flow motions of recirculation, large structure oscillation, and random turbulence. The oscillation frequency of vortex shedding and the intensity of vortical motion in the wake are usually closely related to the shape of the bluffbody as well as the properties of flow and fluid.[2] The researchers and industries choose varied shapes of bluffbodies, for instance, the circular disk,[3] flat plate,[4] circular cylinder,[5] half-triangular cylinder,[6] V gutter,[7] slit V gutter,[8] and so on, depending on the operational purposes. The V-shaped bluffbody, which is conventionally called the V gutter, is usually adopted in many of the combustion apparatuses (e.g., the ramjet combustors, thrust augmenters, industrial burners, etc.), due to its effective flame-holding ability and low pressure-loss characteristics.[9] Dimensionless parameters, such as the Reynolds number, Strouhal

number, and Roshko number, are conventionally employed by the investigators to characterize the flow motions in the bluffbody wake.[10] The average and dynamic wake structures, physical mechanisms, and the applications of the bluffbody wake have attracted the interest of many investigators during the past few decades. Researchers also sought flow control methods of augmenting the momentum and mass exchange rate in the wake.[11]

The fluidic flowmeter,[12,13] which was invented in 1960s by using the Coanda effect,[14] has been widely studied by investigators[15–17] during the past four decades because of its superior characteristics in flow measurement over the vortex shedding flowmeter. It was recently developed for the measurement of microflow rate.[18] Two general categories of the fluidic flowmeters, the feedback oscillator and the target oscillator, are found in the literature.[19] They are classified according to the geometric configurations and the driving forces needed to attain self-sustained oscillation of a plane jet flow. The feedback oscillator consists of two bypass passages that are connected from the downstream wall to the upstream wall of a two-dimensional chamber through which a plane jet is injected. When the jet is deflected to one side of the chamber due to some instabilities that occur in the flow, the pressure or momentum difference induced by the unbalance of the flowfield in the downstream walls of the chamber is transmitted through the bypass passages from the downstream ports of the passages to the upstream ports and "pushes" the jet to the opposite chamber wall. When this situation happens, the reversed unbalance pressure or momentum difference between the upstream ports pushes the jet back to the wall on the other side. The jet then proceeds with a self-sustained oscillation. Pressure transducers or velocimeters installed at proper locations can convert the oscillation frequency of the jet flow into a flow rate reading after appropriate calibration. The target oscillator usually possesses a blockage enclosed in a horseshoe-shaped chamber. The blockage has a crescent surface facing toward the upstream jet inlet. The jet flow is injected into the horseshoe-shaped chamber and impinges the crescent surface of the blockage. The jet undergoes a periodic transverse oscillation if the jet Reynolds number exceeds a critical value.

Some theoretical works have been established to demonstrate the principles of jet oscillation in the target oscillator. Huang[20] employed a classic nonlinear oscillation equation, the Van der Pol equation,[21] to roughly describe this type of jet oscillation. The oscillation behaviors predicted by his model at different Reynolds numbers are in good agreement with those obtained by experiments. Lalanne et al.[22] studied a confined jet impinging a bluffbody. Their work showed that the flow oscillates through a Hopf bifurcation, a periodic nonsymmetric state, when the Reynolds number is larger than a critical value. This state of equilibrium defines a limit cycle characterized by an oscillation frequency and a saturated amplitude.

Uzol and Camci[23] and Camci and Herr[24] have introduced a concept of enhancing the turbulent transport of heat in internal coolant passages of gas-turbine blades by performing computational analysis on a nonenclosed target-type fluidic oscillator. It is found that the target oscillator can produce steady oscillation in a wider range of Reynolds number.

The purpose of this paper is to develop a flow management method based on the fluidic oscillation technique to modulate the flow properties in the near wake of a V-shaped bluffbody. The experimental studies are conducted in a low-speed wind tunnel. The smoke-wire flow visualization technique is used to identify the characteristic oscillation modes and obtain a design criterion of the oscillator. A hot-wire anemometer is employed to detect the oscillation frequency. A two-component laser Doppler velocimeter (LDV) is then used to measure the flow characteristics in the near wake, which is alternatively flushed by the self-sustained oscillating jet. The fluidic oscillation process and the wake properties, which are subjected to the modification of the fluidic oscillation, are presented and discussed.

Experimental Arrangements

Apparatus

The experiments are performed in an open-loop, low-speed wind tunnel with a honeycomb section, three wire-mesh screens, a 10:1 contraction, and a test section of $400 \times 250 \times 1000$ mm, as shown in Fig. 1. Freestream turbulence intensity is lower than 0.4% within the experimental range of $U_\infty = 0.10$–25 m/s, where U_∞ denotes the time-averaged freestream velocity. Nonuniformity of the average velocity profiles across the test section is lower than 0.5%. During the experiments the average velocity of the approaching flow is constantly monitored with a retractable pitot-static tube along with a calibrated Validyne pressure transducer.

Two flat plates, made of Plexiglas® with high transparency, are arranged to form a V-shaped bluffbody with an open leading edge,

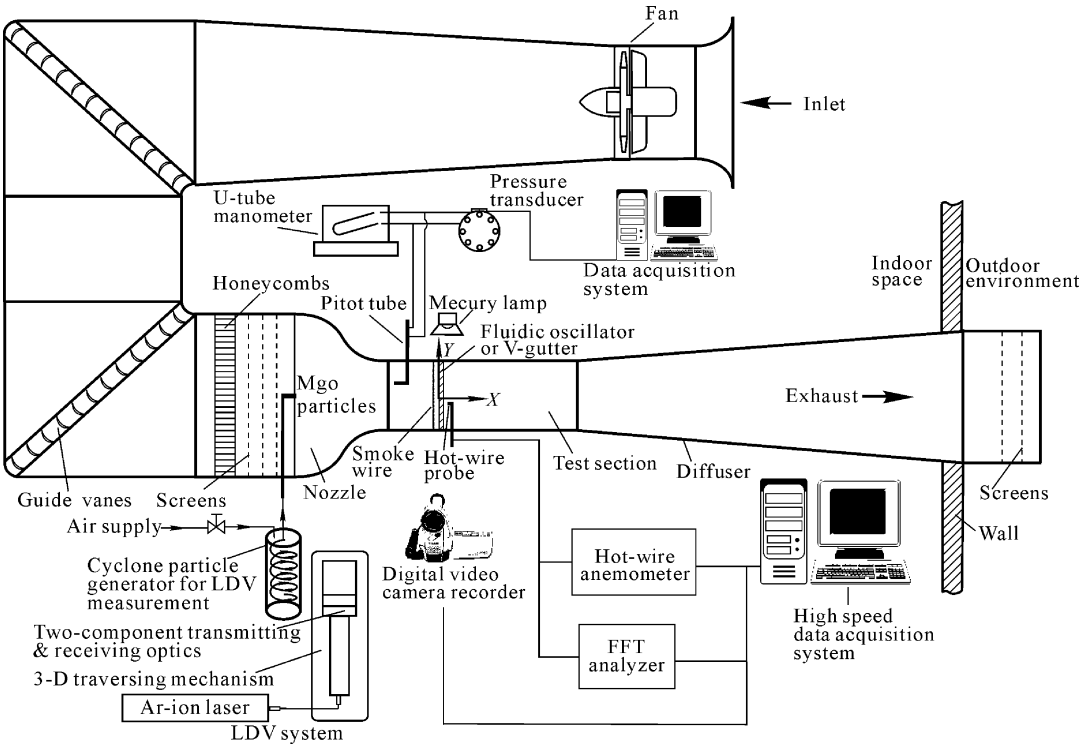

Fig. 1 Experimental setup.

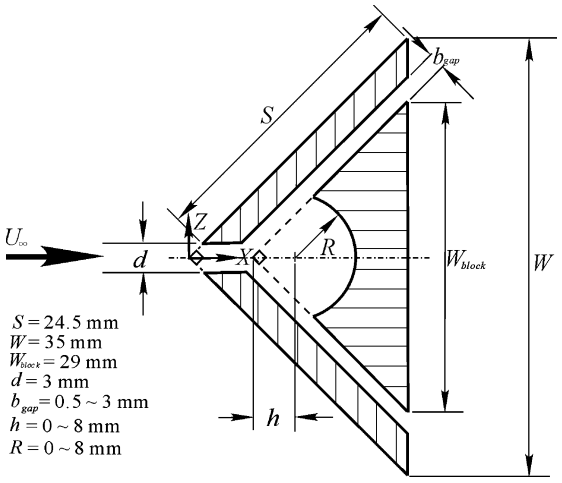

Fig. 2 Geometry of V-shaped fluidic oscillator.

as shown in Fig. 2. The thickness of the flat plates is 3 mm. The transparency of the flat plates allows the transmission of the laser-light sheet for the flow visualization experiment. The V-shaped bluffbody has a span angle of 90 deg, a cross-stream span length $L = 400$ mm, an upstream slit width $d = 3$ mm, and a downstream width $W = 35$ mm. The origin of the reference frame is located at the virtual vertex of the V-shaped bluffbody. The coordinates X, Y, and Z denote the directions in the freestream, span, and cross stream, respectively. A target blockage with a crescent surface facing the upstream slit is placed in the cavity of the V-shaped bluffbody, as shown in Fig. 2. The whole set of devices, which includes the V-shaped bluffbody and the target blockage, is installed horizontally in the cross-stream direction in the test section of the wind tunnel. The vertex of the V-shaped bluffbody is located at a distance of 20 cm downstream of the outlet plane of the wind-tunnel nozzle. It is fixed from two ends by a few small set-screws penetrating through the sidewalls of the test section. The small slit at the leading edge of the V-shaped bluffbody allows the airflow to go through and forms a plane jet in the cavity. The jet impinges the crescent surface of the target blockage. The target blockage has characteristic geometric parameters of h, b_{gap}, and R, as shown in Fig. 2. The crescent profile is a concave arc with a radius R originating from the point located on the symmetry axis at a distance h from the virtual vertex of the triangular target blockage. The symbol R denotes the radius of the crescent profile of the target block; if $R = 0$, the impinging surface becomes flat.

Flow Visualization

The smoke-wire technique is used to visualize the flow oscillation process at low Reynolds numbers. Photography is done via a high-speed charge-coupled device camera. A corrugated wolfram wire with a diameter of 80 μm is used as the smoke-wire. It is placed 10 mm upstream of the leading edge of the V-shaped bluffbody. Thin mineral oil is brush-coated on the wire surface. The wire is ohmically heated to generate fine smoke streaks and thus make the flowfield visible. The surface temperature of the smoke-wire is kept as low as possible but high enough to evaporate the oil. The buoyancy-induced convection[25] is estimated to be lower than 2.5 cm/s. The condensed vapor aerosols (the "smoke") of the thin mineral oil have diameters at an order of magnitude about 1 μm (Ref. 26). The slip factor and Stokes number[27] for these aerosols are estimated to be about 1.108 and 0.002, respectively. The smoke streaks hence are considered to be able to follow the flow appropriately.

Frequency Detection

The frequencies of the jet oscillation and the shed vortices in the wake region are detected by a home-made, constant-temperature, one-component hot-wire anemometer. The output signals of the hot-wire anemometer are fed simultaneously to a fast Fourier transform (FFT) analyzer and a high-speed personal computer–based data acquisition system to execute analysis and calculations of dynamic behavior and flow statistics, as shown in Fig. 1. The data acquisition system has a sample-and-hold function for multichannel acquisition without phase lag. The hot-wire probe used is TSI 1210-T1.5, which can be applied in either the endflow or the crossflow. The original tungsten wire is replaced by platinum wire. The wire diameter and length are 5 μm and 1.5 mm, respectively. The dynamic response corresponding to the electronic square-wave test is adjusted to 20 kHz. The sampling rate and the elapse, time of the data acquisition system are set to 23,000 samples/s and 7 s, respectively, for the measurements of average velocity, turbulence intensity, and wake-instability detection.

Velocity Field Measurements

The velocity fields are measured with a two-component LDV. The blue and green laser beams, which are supplied by a Spectra-Physics Stabilite-2017 6-W argon-ion laser, are separated and focused through the Dantec Fiber-Flow optical system. The dimensions of the measuring volumes of the green and blue components estimated at e^{-2} light-intensity level are about $0.120 \times 0.120 \times 1.543$ and $0.114 \times 0.114 \times 1.463$ mm, respectively. The fringe separations of these components are 3.31 and 3.14 μm, respectively. The system is configured to operate in backscatter mode. A Bragg cell is embedded in the system to distinguish the directional ambiguity. A Dantec flow velocity analyzer enhanced two-component correlation processor is used to convert the Doppler signals into frequency data. The frequency data are fed into a personal computer–controlled data acquisition system to calculate the velocities and other statistical properties. The length of each velocity data record is 10,000 samples and the elapse time is about 2 s, so that the average sampling rate is about 5 kHz. By taking the maximum vortex shedding frequency in the wake about 200 Hz, approximately 25 cycles of the wake dynamic structures would be captured in a data record for calculations of average and turbulence properties. The transmitting/receiving optics of the LDV are installed and precisely mounted on a three-component traversing mechanism for spatial positioning. The resolution of the traversing mechanism is 10 μm.

Magnesium oxide particles with an average diameter of 5 μm are introduced into the flow to scatter the laser light via two cyclone particle seeders. The cyclone particle seeders, which are similar to that described by Glass and Kennedy,[28] are made in-house. The particles are estimated to be capable of following frequencies up to 3.6 kHz (Ref. 29).

Uncertainties

The accuracy of freestream velocity measurement is primarily affected by the alignment of the pitot tube and the calibration of the pressure transducer. With the help of an online micropressure calibration system and careful alignment of the pitot tube, the uncertainty of the freestream velocity is estimated to be as large as 3% of the reading. The alignment mechanism for the V-shaped blockage has a resolution of 0.2 deg. The accuracy of measuring the fluidic oscillation and the vortex shedding frequencies depends not only on the response of the hot-wire anemometer but also on the record length and the sampling rate of the FFT analyzer. The uncertainty of the detected frequency is estimated to be within 1.5% of reading in this experiment. The estimated uncertainties of the LDV measurements are less than 1% for the mean velocities and 7% for the turbulence intensities and Reynolds stresses.

Results and Discussion

To find the conditions that the stable, periodic fluidic oscillations can sustain, many oscillators with different geometries are tested at various Reynolds numbers. As shown in Fig. 2, important geometric dimensions of the V-shaped fluidic oscillator employed in the study are summarized as follows: 1) width of the leading-edge slit $d = 3$ mm; 2) downstream width of the V-shaped bluffbody $W = 35$ mm; 3) thickness of the V-shaped bluffbody side plates, 3 mm; 4) gap between the side-plate and the target blockage $b_{\text{gap}} = 0.5$, 1, 2, 3 mm; 5) offset distance from the crescent origin to the virtual vertex of the target blockage $h = 0, \ldots, 8$ mm; and 6) radius of the crescent profile $R = 0, \ldots, 8$ mm. Because

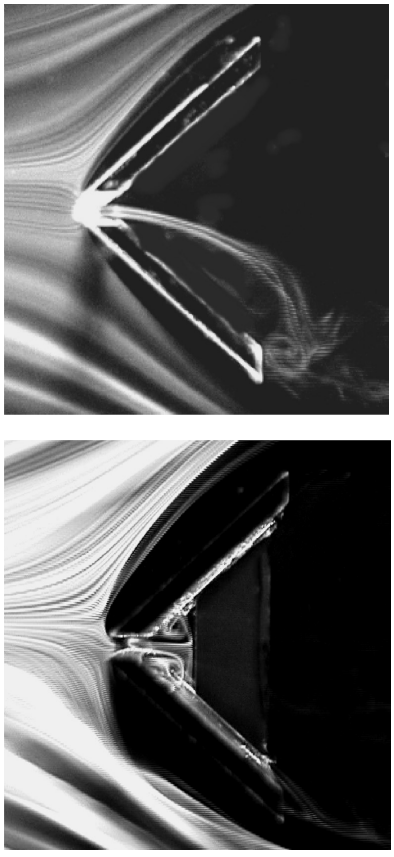

Fig. 3 Smoke-streak flow patterns in oscillator cavity: a) slit V gutter, $Re_d = 339$, $Re_W = 3955$; and b) flat-surface target blockage, $Re_d = 436$, $Re_W = 5.09 \times 10^3$, $b_{gap} = 1$ mm, $R = 0$; shutter speed = 1/2000 s.

the vortex shedding in a bluffbody wake is closely related to the width of projection of the bluffbody on the cross-stream plane,[10] the Reynolds number based on the downstream width W of the V-shaped bluffbody, Re_W, is used to describe the oscillation motions in the wake. The Reynolds number Re_d, which is based on slit width d and freestream velocity U_∞, is used to characterize the fluidic oscillation inside the oscillator because the fluidic oscillation is commonly characterized by the jet Reynolds number.[15–20] The Reynolds number Re_W, which is based on the cross-stream width W and the freestream velocity U_∞, ranges from 2.3×10^3 to 6.0×10^4 in this study. In terms of Re_d, it goes approximately from 200 to 5.2×10^3.

Smoke-Streak Flow Patterns

Slit V Gutter and Flat Impinging Surface

Figure 3a shows the smoke-streak flow pattern in the slit V gutter. The width d of the slit at the leading edge of the V gutter is 3 mm. The approaching flow going through the slit at the leading edge deflects toward one side of the V-gutter wing and forms a recirculation bubble due to the Coanda effect. The deflected slit jet does not oscillate back and forth between the two wings of the slit V gutter. If the flow is subject to a perturbation or if the wind tunnel is shut down and restarted, the slit jet may deflect to the other side.

If a block with a flat surface is installed in the slit V-gutter cavity, as shown in Fig. 3b, part of the approaching flow goes through the slit, impinges the flat target surface of the block, bifurcates into two streams, and forms two standing counter-rotating vortices. The block with a flat target surface is a special case ($R = 0$) of the crescent surface ($R > 0$).

Crescent Impinging Surface

When $R > 0$, the slit jet and the flows in the crescent cavity present four characteristic modes at different combinations of h and R. Figure 4 shows the typical smoke-wire flow patterns of these flow modes. The deflection mode, as shown in Fig. 4a, is usually

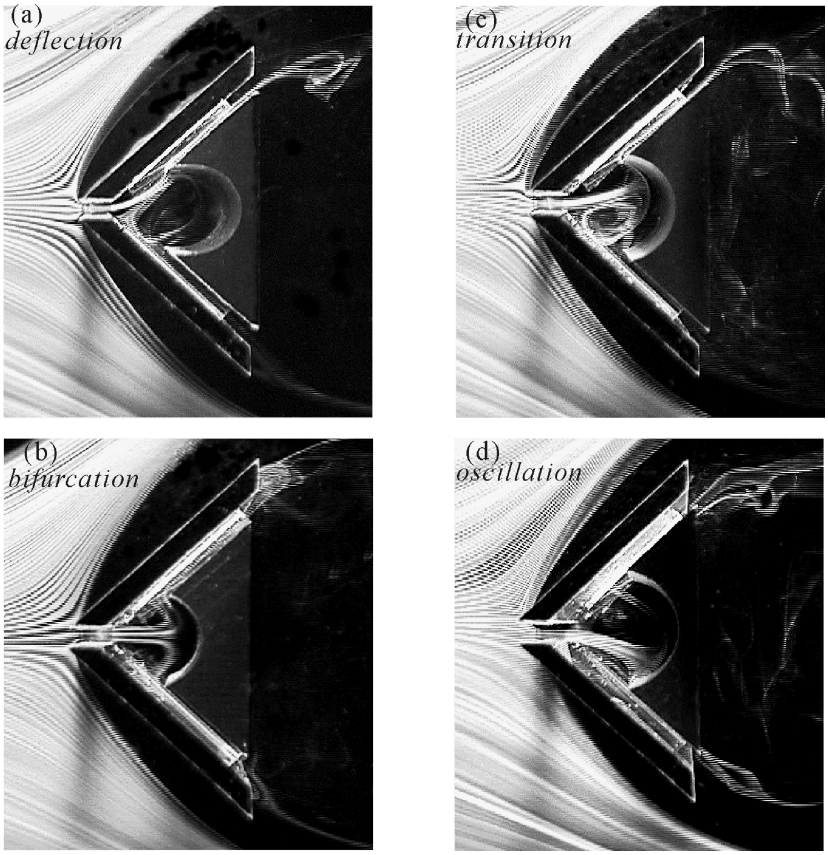

Fig. 4 Smoke-streak flow patterns in cavity of V-shaped fluidic oscillator ($Re_d = 260$, $Re_W = 3.036 \times 10^3$, $b_{gap} = 2$ mm): a) deflection mode, $h/d = 2.67$, $R/d = 2$; b) bifurcation mode, $h/d = 1$, $R/d = 2.33$; c) transition mode, $h/d = 1.67$, $R/d = 2.33$; and d) oscillation mode, $h/d = 2$, $R/d = 2.67$; shutter speed = 1/2000 s.

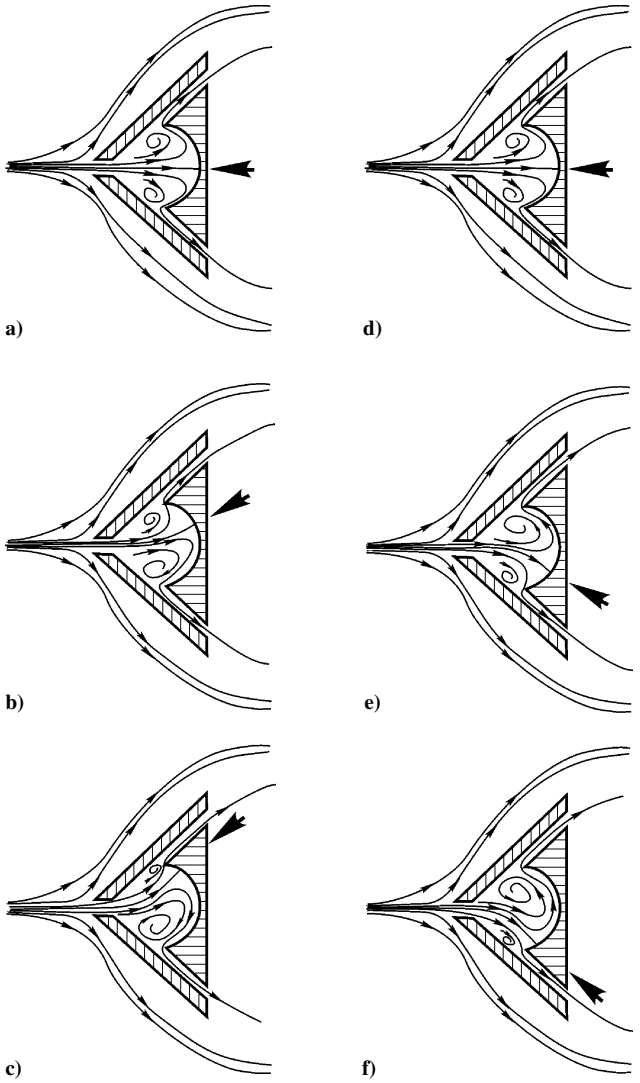

Fig. 5 Sketches delineating typical oscillation process of oscillation mode.

found at large values of h/d. The slit jet in the crescent cavity is deflected from the central symmetry axis and attached to the inner wall of one of the V-gutter walls. No transverse oscillation of the jet is found. Most of the space in the cavity is occupied by a large clockwise-rotating vortex. At low values of h/d, the bifurcation mode is found, as shown in Fig. 4b. The slit jet impinges the crescent surface of the target block and bifurcates toward the V-gutter side plates. Two standing counter-rotating vortices similar to those observed in Fig. 3b are formed in the crescent cavity. At some proper values of h/d and R/d, the slit jet oscillates intermittently, which is called the transition mode. Figure 3c shows the smoke flow pattern at intermediate instance when the jet oscillates intermittently. The intermittent oscillation is not periodic. When h/d and R/d slightly change to some proper values, the intermittent oscillation motion of the slit jet becomes periodic and stable, which is called the oscillation mode. Figure 4d shows the smoke pattern of the oscillation mode at the instance that the oscillating jet is moving toward the lower sideplate of the V-shaped bluffbody. Sketches delineating the typical sequential motions of the flows in the oscillation mode are shown in Figs. 5a–5f. They are simulated from the video animation of the smoke-streak patterns. In Fig. 5a the slit jet is located at the neutral position. Two counter-rotating vortices are induced in the cavity due to the topological reasoning. The slit jet swings toward the upper wall, as shown in Figs. 5b and 5c. The upper vortex shrinks and the lower one swells gradually during the swing-up process. When the slit jet swings up, air in the upper bubble is pushed out of the chamber, passes through the upper gap, and emerges from the opening in the downstream face of the V gutter. The slit jet swings back to the neutral position in Fig. 5d and proceeds toward the lower wall in Figs. 5c and 5d.

Characteristic Flow Regimes

The characteristic flow modes are closely related to the values of the Reynolds number Re_d, the offset distance from the crescent origin to the virtual vertex of the target block h, and the radius of the crescent profile R. Figure 6 shows typical characteristic regimes of flow modes at various Reynolds numbers at $b_{\text{gap}} = 1$ mm. The narrow bands that are composed of short slashes represent the boundaries between different characteristic flow modes. The data for the boundaries between different flow regimes are obtained from observing the animation of the smoke-wire flow images. The coordinates of h and R are normalized by the slit width d. The deflection mode occurs when h/d is larger than about 1.5 if $R/d = 1.7$. The larger the value of R/d, the higher the value of h/d that is required to observe the deflection mode. The lower limit of h/d for the occurrence of deflection mode does not change significantly with the Reynolds number. Roughly speaking, when $h/d > 1.22(R/d) - 0.57$, the deflection mode occurs. The bifurcation mode is observed at low values of h/d. In general, the bifurcation mode occurs when $h/d < -1.23(R/d) + 4$ for $R/d > 1.9$.

The stable oscillation mode occurs in a triangular regime on the domain of $(h/d, R/d)$. The regime of the stable oscillation jet enlarges with the increase of Reynolds number, as shown in Fig. 6.

Figure 7 shows the collections of the boundaries of the oscillation mode at various Reynolds numbers. At $h/d > 1.67$, the slopes of the boundaries are positive. At $h/d < 1.67$, the slopes of boundaries are negative. To obtain established, self-sustained fluidic oscillation, the values of h/d, R/d, and Re_d have to fall within the regime that is confined by the boundaries described by the following fitted equations:

$$(h/d)_{\substack{\text{upper}\\\text{boundary}}} = \left(-1.72 \times 10^{-6} Re_d^2 + 1.57 \times 10^{-3} Re_d + 0.29\right) \times \exp\left[\left(9.42 \times 10^{-9} Re_d^3 - 1.01 \times 10^{-5} Re_d^2 + 3.29 \times 10^{-3} Re_d + 0.17\right)(R/d)\right], \qquad h/d > 1.67 \tag{1}$$

$$(h/d)_{\substack{\text{lower}\\\text{boundary}}} = \left(2.29 \times 10^{-5} Re_d^2 - 1.22 \times 10^{-2} Re_d + 12.14\right) \times \exp\left[\left(4.54 \times 10^{-9} Re_d^3 - 6.53 \times 10^{-6} Re_d^2 + 2.18 \times 10^{-3} Re_d - 1.04\right)(R/d)\right], \qquad h/d < 1.67 \tag{2}$$

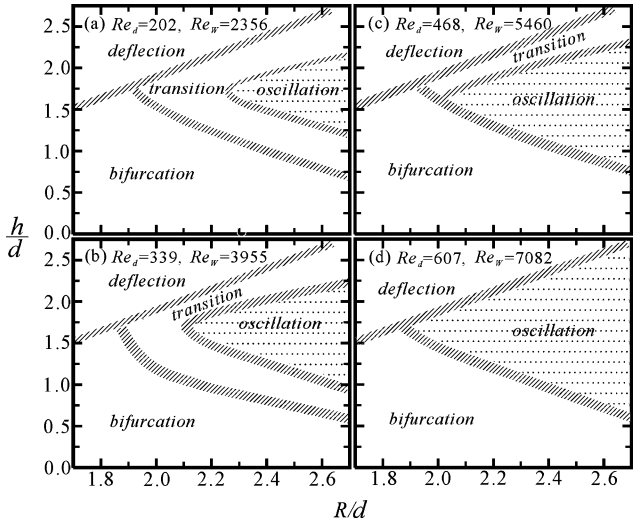

Fig. 6 Characteristic regimes of V-shaped fluidic oscillation (b_{gap} = 1 mm): a) $Re_d = 202$, $Re_W = 2.357 \times 10^3$; b) $Re_d = 339$, $Re_W = 3.955 \times 10^3$; c) $Re_d = 468$, $Re_W = 5.46 \times 10^3$; and d) $Re_d = 607$, $Re_W = 7.082 \times 10^3$.

Oscillation Frequencies

Figures 8a–8d show the instantaneous velocity signals and the corresponding power spectrum density functions in the wake of a closed-tip V gutter. Figures 8e–8h show the oscillation signals and the power spectrum density functions in the wake of the fluidic oscillator. In Fig. 8, the symbol U denotes the local instantaneous velocity measured by the one-component hot-wire anemometer, f_s represents the frequency of vortex shedding in the wake of the V-shaped bluffbody, f_f is the frequency of fluidic oscillation, and Φ is the power spectrum density function obtained from the fluctuation velocity. The results of the slit V gutter are not shown here because the vortex shedding frequencies are the same as those of the corresponding closed-tip V gutter. The data are obtained from measurements of a hot-wire anemometer. The closed-tip V-gutter wake consists of signals of shedding vortices with a frequency $f_s = 36$ Hz at $Re_w = 1.5866 \times 10^4$ ($Re_d = 1.36 \times 10^3$) and $f_s = 96$ Hz at $Re_w = 4.2537 \times 10^4$ ($Re_d = 3.65 \times 10^3$). The periodically oscillating velocity signals are superimposed by fairly turbulent fluctuations. The wake of the fluidic oscillator presents two characteristic frequencies. One is the vortex shedding frequency f_s, which is the same as that measured in the wake of the closed-tip V gutter, that is, $f_s = 36$ Hz at $Re_w = 1.5866 \times 10^4$ ($Re_d = 1.36 \times 10^3$) and $f_s = 96$ Hz at $Re_w = 4.2537 \times 10^4$ ($Re_d = 3.650 \times 10^3$). The other one, which is called the fluidic oscillation frequency f_f, is significantly larger than the vortex shedding frequency f_s; for example, $f_f = 1030$ Hz at $Re_w = 1.5866 \times 10^4$ ($Re_d = 1.36 \times 10^3$) and $f_f = 3206$ Hz at $Re_w = 4.2537 \times 10^4$ ($Re_d = 3.65 \times 10^3$). They are induced by the periodic emergence of the oscillation slit-jet from the downstream opening of the oscillator.

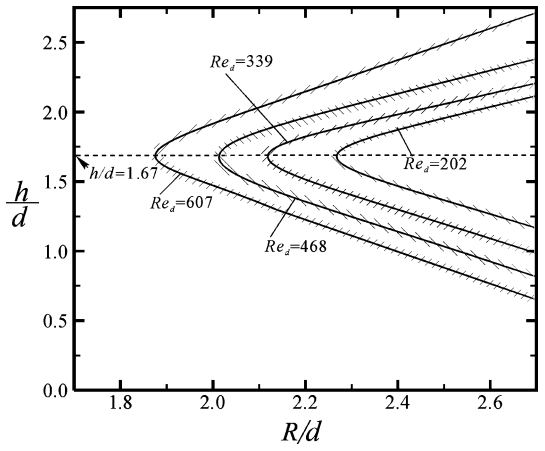

Fig. 7 Collection of boundaries of oscillation mode at various Reynolds numbers.

The frequencies of the vortex shedding and fluidic oscillation increase linearly with the increase of the freestream velocity, as shown in Fig. 9. The frequency of fluidic oscillation in general is about 25 to 40 times higher than its counterpart of vortex shedding. It is found in this study that setting b_{gap} at 1 mm can attain the best results of oscillation, that is, the largest oscillation frequency and amplitude. For the gap width smaller than 1 mm, the oscillation disappears very fast with the decrease of b_{gap}. It is probably because large flow resistance is experienced in the narrow passages when b_{gap} is small. For the cases when $b_{\text{gap}} > 1$ mm, both the fluidic oscillation frequency and the strength of oscillation decrease with the increase of the gap width.

Figure 10 shows the normalized frequencies, the Strouhal numbers of the vortex shedding, and the fluidic oscillation. The Strouhal numbers $Sr_{d,f}$, $Sr_{W,f}$, and $Sr_{W,s}$ are defined as $f_f \times d/U_\infty$, $f_f \times W/U_\infty$, and $f_s \times W/U_\infty$, respectively. The first subscript, W or d, in the symbols $Sr_{W,f}$, $Sr_{W,s}$, and $Sr_{d,f}$ denotes the length scale used for the calculation of Strouhal number. The second subscript, f or s, denotes that the frequency used for the calculation of Strouhal numbers is f_f or f_s. In the lower part of Fig. 10, all Strouhal numbers $Sr_{W,s}$ of the vortex shedding collapse to a constant value of about 0.182 when Re_W is greater than about 4000, which coincides with the previous results for the closed-tip V gutter by Yang et al.[8] However, the Strouhal numbers $Sr_{W,f}$ or $Sr_{d,f}$ of the

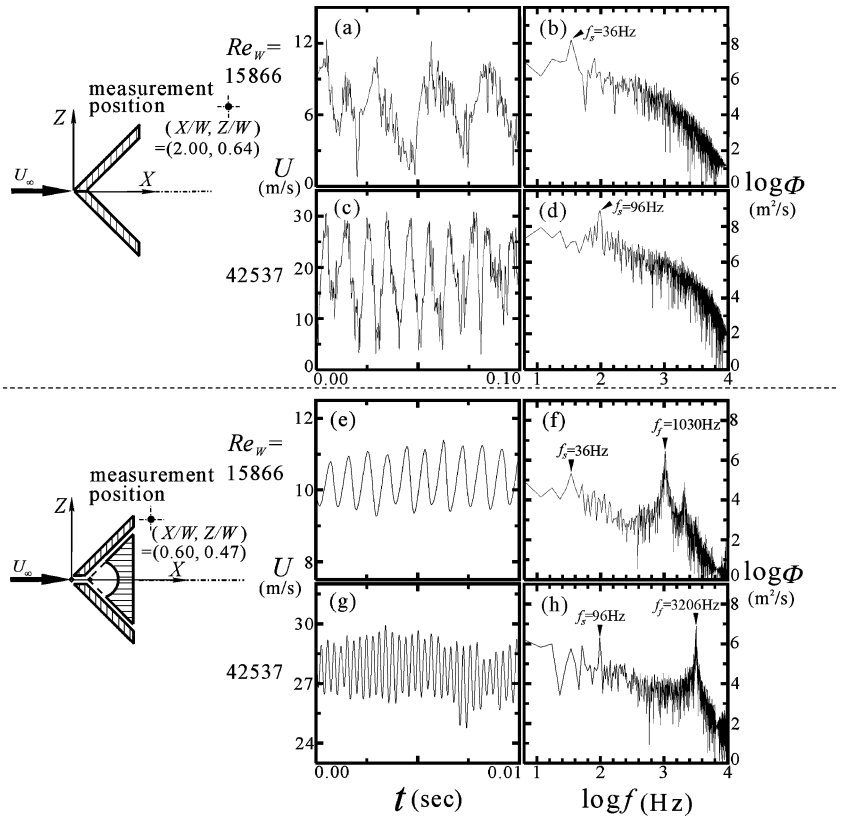

Fig. 8 Instantaneous oscillating velocity signals (a, c, e, g) and corresponding power spectrum density functions of fluctuating velocities (b, d, f, h) of hot-wire anemometer output: a–d) closed-tip V gutter and e–h) V-shaped fluidic oscillator (b_{gap} = 1 mm, h/d = 2, R/d = 2.67).

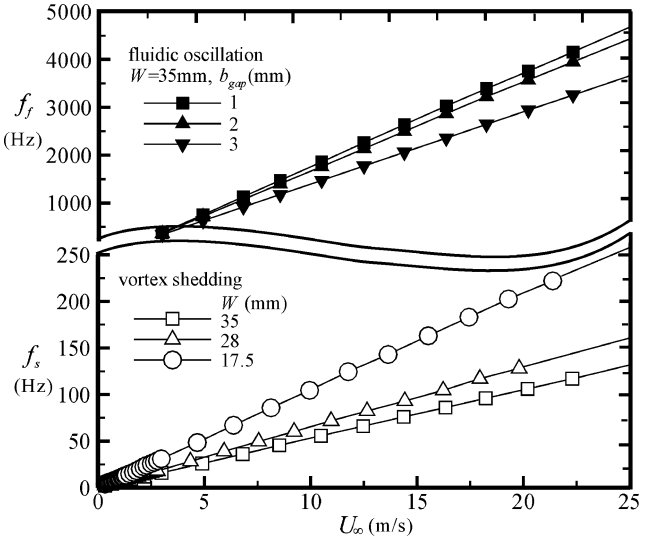

Fig. 9 Vortex shedding frequencies of closed-tip V gutter and fluidic oscillation frequencies of V-shaped fluidic oscillator (b_{gap} = 1 mm, h/d = 2, R/d = 2.67).

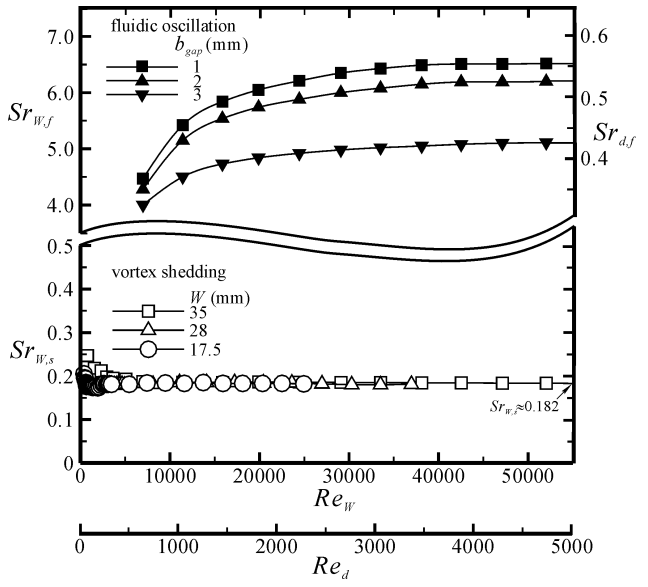

Fig. 10 Strouhal numbers of vortex shedding and fluidic oscillation frequencies of V-shaped fluidic oscillator (b_{gap} = 1 mm, h/d = 2, R/d = 2.67.

fluidic oscillations at different gap widths b_{gap} do not correlate to a single curve. For a certain gap width, the Strouhal number of the fluidic oscillation increases with the increase of Reynolds number at a fast rate when $Re_d < 2.0 \times 10^3$, then the increase rate drops gradually. At large Reynolds numbers, it would approach a constant. For instance, $Sr_{d,f}$ of the fluidic oscillation would approach about 0.56 at large Reynolds numbers at $b_{gap} = 1$ mm. The oscillation Strouhal number $Sr_{d,f}$ of the presently developed oscillator is about 80 times larger than the previous results for the enhancement of heat transfer ($f_f = 28$ Hz and $Sr_{d,f} = 0.007$ at $Re_d = 5.0 \times 10^3$)[23,24] and about 60 times larger than that for the fluidic flowmeter ($f_f = 500$ Hz and $Sr_{d,f} = 0.009$ at $Re_d = 5.0 \times 10^3$).[22] The differences may be brought up from the optimized design of the geometry of the oscillation chamber.

Streamline Patterns and Characteristic Lengths

By using the two-component LDV, the velocity fields at various Reynolds numbers $Re_w = 6.533 \times 10^3$, 1.0966×10^4, 1.54×10^4, and 1.87×10^4 are measured. Figure 11 shows the time-averaged streamline patterns at $Re_w = 10{,}966$. In the near-wake region of the

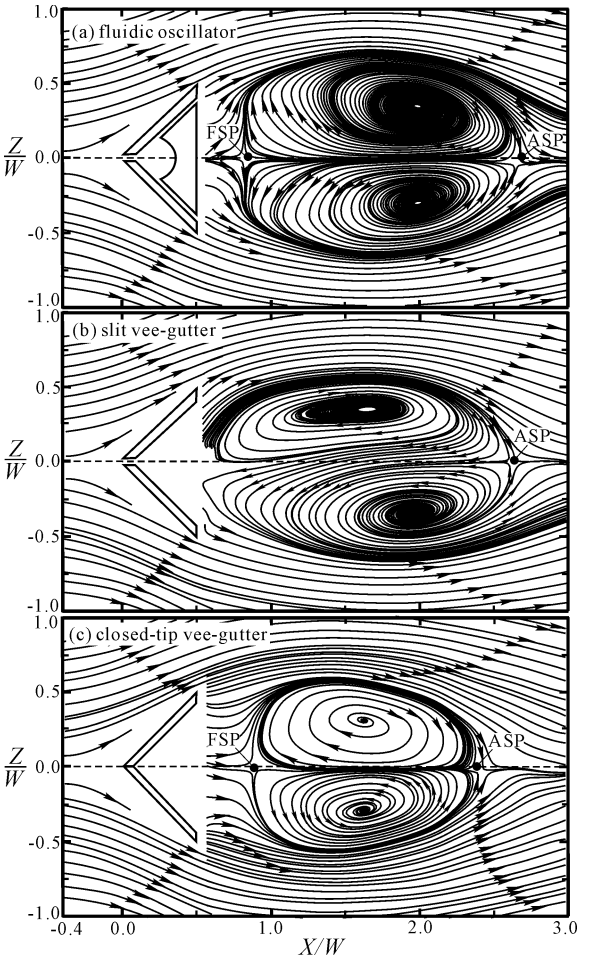

Fig. 11 Streamline patterns in the near wakes of a) fluidic oscillator, b) slit V gutter, and c) closed-tip V gutter (Re_W = 10,966).

fluidic oscillator, as shown in Fig. 11a, a recirculation bubble, which is almost symmetric about the central axis, exists in between two four-way saddles.[30] The four-way saddles, which are designated by ASP (aft stagnation point) and FSP (forward stagnation point), are located on the central axis at $X/W \approx 2.65$ and 0.85, respectively. The axial length of the recirculation bubble is thus about 1.8 W. The maximum cross-stream width of the recirculation bubble in Fig. 11a is about 1.42 W. In Fig. 11b for the slit V gutter, the recirculation bubble is asymmetric about the central axis due to the upward deflection of the jet when the flow goes through the slit of the V gutter. The aft stagnation point is identified at $X/W \approx 2.62$, which is about the same location as that in Fig. 11a. The FSP is not shown because the measurements are not extended upstream into the slit V gutter. It is apparent that the bubble length of the fluidic oscillator would be larger than that of the slit V gutter if the forward stagnation point does exist inside the slit V gutter. For the closed-tip V gutter, as shown in Fig. 11c, the near-wake flow structure is similar to that of the fluidic oscillator: a recirculation bubble, which is almost symmetric about the central axis, exists in between two four-way saddles. The axial bubble length in Fig. 11c is about 1.45 W, which is much shorter than that of the fluidic oscillator in Fig. 11a because the ASP moves upstream and the FSP moves downstream in the case of the closed-tip V gutter. The maximum cross-stream width of the recirculation bubble in Fig. 11c is about 1.18 W, which is much smaller than that in Fig. 11a. In the flowfield of the fluidic oscillator, the alternative injection of the momentum and mass into the near-wake region via the self-sustained oscillating jets may be the primary factor that causes the recirculation bubble to swell to a larger size than its counterpart of the closed-tip V gutter.

The normalized axial distances X_{ASP}/W of the ASP of recirculation bubble behind the V-shaped bluffbodies decrease almost

linearly with the increase of Reynolds number, as shown in Fig. 12. The ASPs of bubble structures of the fluidic oscillator and the slit V gutter do not deviate significantly from each other at larger Reynolds numbers and are about 0.3 W downstream of the ASP of the corresponding bubble structure of the closed-tip V gutter. The bubble lengths of the fluidic oscillator and the closed-tip V gutter are constants of about 1.8 and 1.45, respectively, at all Reynolds numbers tested in this study.

Velocity Distributions

The normalized time-averaged X-component velocity profiles, $\bar{u}/U_\infty$, of the fluidic oscillator, the slit V gutter, and the closed-tip V gutter at various downstream stages in the near-wake region are shown in Fig. 13. The symbol $\bar{u}$ denotes the local averaged velocity in the X direction measured by LDV. The fluidic oscillator is operated in oscillation mode. At the stage $X/W = 0.6$, which is just behind the V gutter, the velocity profiles $\bar{u}/U_\infty$ of the fluidic oscillator and the closed-tip V gutter are symmetric about $z/W = 0$ and negligibly small in the region $-0.5 < Z/W < 0.5$. The velocity profile of the slit V gutter at the stage $X/W = 0.6$ is asymmetric about the central axis and has values larger than the other two types of V-shaped bluffbodies in the region $0.25 < Z/W < 0.5$. Outside the wake region around the shear layers, the velocity of the fluidic oscillator is larger than that of other blockages. This velocity increase in the shear layers may be induced from the oscillating slit jet emerging from the openings of the oscillator. In the region where $|Z/W|$ is greater than about 2, which is not shown in the plot, all velocity profiles approach the freestream velocity. At the stages $X/W = 1.0$ and 1.5, the $\bar{u}/U_\infty$ velocities are negative in the lee-side region of the bluffbody because the measurements are in the recirculation bubble. The asymmetry of the velocity profiles of the slit V gutter at the downstream stage is not as obvious as that at the upstream stage, $X/W = 0.6$. At the stage $X/W = 3.0$, which is downstream of the ASP, the "flat" velocity defect in the near wake of $X/W = 1$ evolves to a concave profile. The values of $\bar{u}/U_\infty$ in the wake of the fluidic oscillator are generally a little greater than those of other V-shaped bluffbodies.

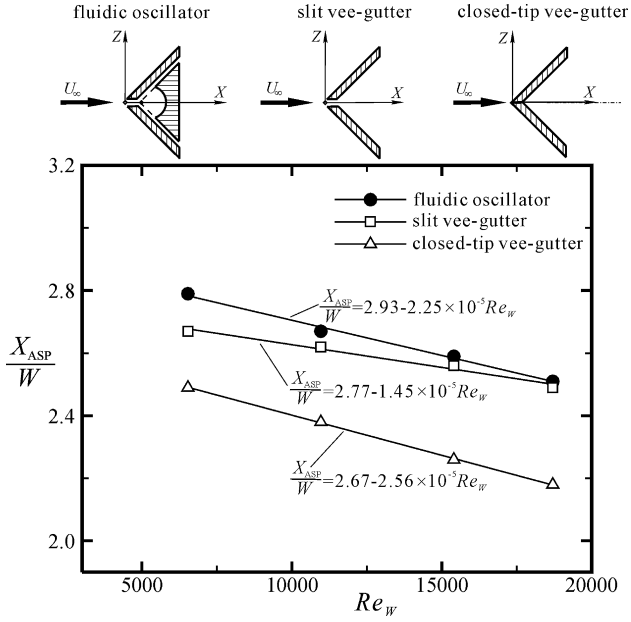

Fig. 12 Normalized axial locations of aft stagnation point.

Turbulence Characteristics

Figure 14 shows the cross-stream distributions of the X-component turbulence intensity T_u in the near-wake regions of the fluidic oscillator, the slit V gutter, and the closed-tip V gutter at various downstream stages in the near-wake region. The turbulence intensity is defined as $T_u \equiv u'/U_\infty$, where u' is the root mean square of the fluctuating velocity $\{=\sqrt{[\sum_n (u - \bar{u}^2)/n]}\}$, in which u denotes the instantaneous velocity and n is the number of data points in the collected data record).

At the stage $X/W = 0.6$, the turbulence intensities in the wake of the closed-tip V gutter are about 8% in the region $-0.5 < Z/W < 0.5$. The slit V gutter has particularly large fluctuation intensities (maximum at about 18%) in the region of Coanda-effect induced jet deflection. In other regions in the wake, the turbulence intensities are about the same level (about 12%) as that of the fluidic oscillator. In the regions $0.5 < |Z/W| < 0.7$, peak turbulence intensities appear behind the fluidic oscillator because of the periodic emergence of the slit jet from the opening of the oscillator. The peak value of the turbulence intensity can reach up to about 17%.

At the stage $X/W = 1.0$ (in the recirculation bubble), the turbulence intensities in the shear layers of the fluidic oscillator are

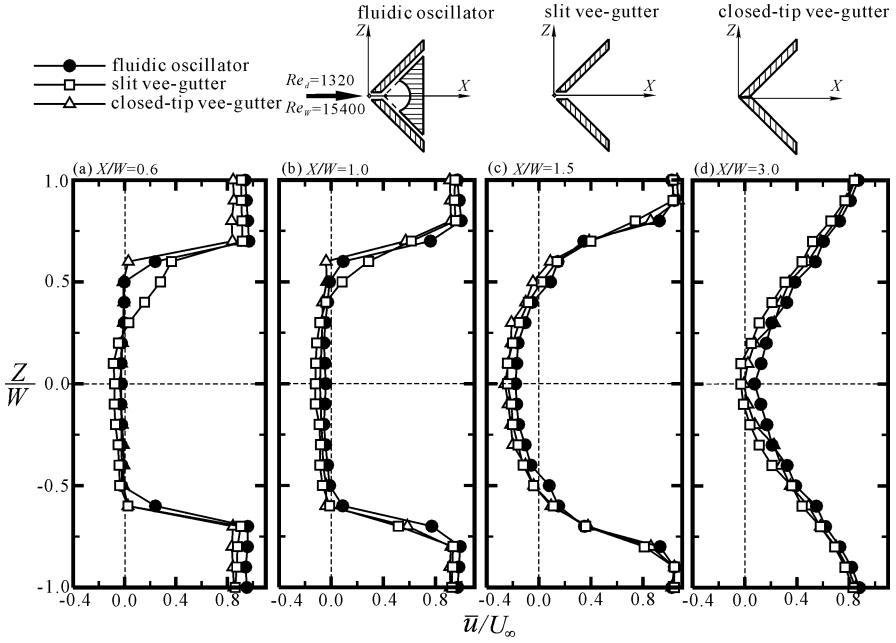

Fig. 13 Normalized time-averaged velocity profiles of X component in the wake of fluidic oscillator, slit V gutter, and closed-tip V gutter (Re_d = 1.32 × 10^3, Re_W = 1.54 × 10^4, b_{gap} = 1 mm, h/d = 2, R/d = 2.67).

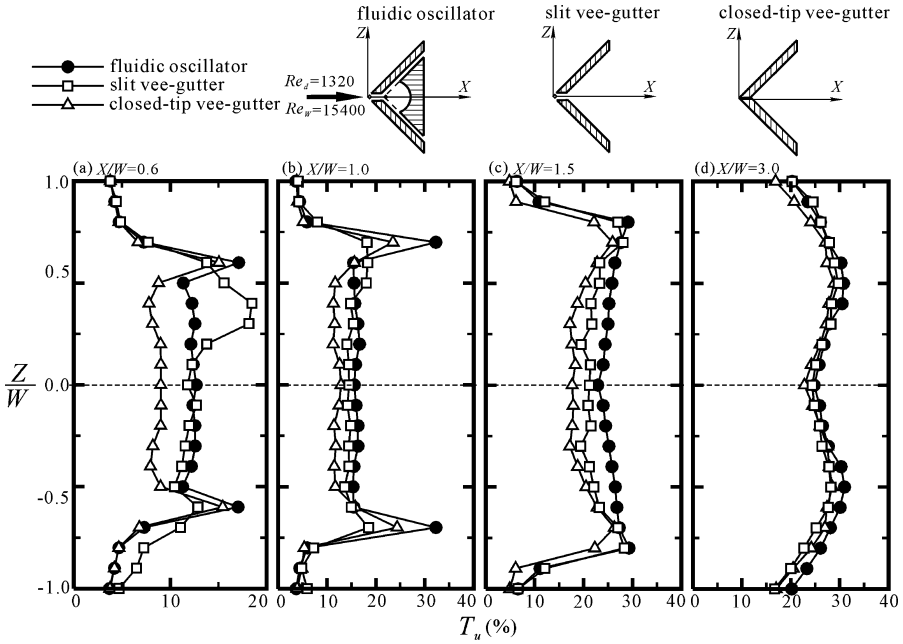

Fig. 14 Turbulence intensity distributions of u velocity in the wake of fluidic oscillator, slit V gutter, and closed-tip V gutter ($Re_d = 1.32 \times 10^3$, $Re_W = 1.54 \times 10^4$, $b_{gap} = 1$ mm, $h/d = 2$, $R/d = 2.67$).

prominently higher than those of the other two bluffbodies. Peak values of the turbulence intensities in the shear layers of the fluidic oscillator may attain about 32%. In the wake, the turbulence intensities of the fluidic oscillator, slit V gutter, and closed-tip V gutter are about the levels of 17, 14, and 12%, respectively. At the stage $X/W = 1.5$, which is still in the recirculation bubble, T_u profiles in the wakes of the fluidic oscillator, slit V gutter, and closed-tip V gutter increase by about 7% to higher levels of about 25, 21, and 18%, respectively. However, the turbulence intensities in the shear layers of the fluidic oscillator are no longer significantly larger than those of the slit V gutter. In the fluidic oscillator, the kinetic energy of the self-sustained oscillatory slit jets injecting into the near-wake region seems to be effectively converted to turbulence kinetic energy in the recirculation bubble. Downstream of the recirculation bubble, as shown in Fig. 14d for $X/W = 3.0$, the turbulence intensities of all three V-shaped bluffbodies present similar levels without significant difference, although those of the fluidic oscillator are a little larger.

Summary

A flow control method by using the principle of a fluidic oscillator is developed for the V-shaped bluffbody flows. The dynamic behaviors of the fluidic oscillations, the frequency characteristics in the fluidic chamber and in the wake, as well as the turbulence properties of the fluidic oscillator, slit V gutter, and closed-tip V gutter, are measured and analyzed. The following conclusions are drawn from the results and discussion:

1) Inserting a target block with a specially designed crescent surface into the cavity of the slit V gutter may induce self-sustained, periodic fluidic oscillations. By directing the fluidic oscillation to the near-wake region, the flow properties can be significantly modulated. Parameters influencing the fluidic oscillations include the offset distance from the crescent origin to the virtual vertex of the target block, the radius of the crescent profile of the target block, and the Reynolds number. For future work, computational fluid dynamics may be of assistance in the optimization process of this device.

2) The oscillating motions in the wake region of the fluidic oscillator contain two types of instabilities: the high-frequency fluidic oscillation and the low-frequency vortex shedding. The vortex shedding frequencies are the same as the corresponding closed-tip V gutter and the slit V gutter. The high-frequency oscillations induced by the dynamic Coanda effect which are superimposed on the signals of the shed vortices, may serve as an oscillatory triggering source. The Strouhal number of the self-sustained oscillations of current geometric configuration may attain a value of about 0.56 at large Reynolds numbers, which is much higher than the conventional ones used for heat transfer enhancement and fluidic flowmeter.

3) Compared with the closed-tip and slit V gutters, the turbulence intensities around the edge and in the wake of the fluidic oscillator are significantly increased because the kinetic energy of the self-sustained oscillatory slit jets injecting into the near-wake region of the fluidic oscillator seems to be effectively converted to the turbulence kinetic energy in the recirculation bubble. The increased turbulence level in the wake may suggest the application of this device in the cases that require enhancement of mixing and/or combustion efficiency, for example, the industrial combustors and the afterburners of the jet-engine combustors.

References

[1]Tritton, D. J., *Physical Fluid Dynamics*, 2nd ed., Oxford Univ. Press, Oxford, 1988, pp. 123–151.

[2]Roshko, A., "On the Wake and Drag of Bluff Bodies," *Journal of the Aerospace Sciences*, Vol. 22, Feb. 1955, pp. 124–135.

[3]Huang, R. F., and Lin, C. L., "Characteristic Modes and Thermal Structure of Nonpremixed Circular-Disc Stabilized Flames," *Combustion Science and Technology*, Vol. 100, Nos. 1–6, 1994, pp. 123–139.

[4]Popiel, C. O., and Turner, J. T., "Visualization of High Blockage Flow Behind a Flat Plate in a Rectangular Channel," *Journal of Fluids Engineering*, Vol. 113, No. 1, 1991, pp. 143–146.

[5]Hertzberg, J. R., Shepherd, I. G., and Talbot, L., "Vortex Shedding Behind Rod Stabilized Flames," *Combustion and Flame*, Vol. 86, No. 1, 1991, pp. 1–11.

[6]Fujii, S., Gomi, M., and Eguchi, K., "Cold Flow Tests of a Bluff-Body Flame Stabilizer," *Journal of Fluids Engineering*, Vol. 100, No. 2, 1981, pp. 323–332.

[7]Stwalley, R. M., and Lefebvre, A. H., "Flame Stabilization Using Large Flameholders of Irregular Shape," *Journal of Propulsion*, Vol. 4, No. 1, 1988, pp. 4–13.

[8]Yang, J. T., Yen, C. W., and Tsai, G. L., "Flame Stabilization in the Wake Flow Behind a Slit V-Gutter," *Combustion and Flame*, Vol. 99, No. 2, 1994, pp. 288–294.

[9]Lefebvre, A. H., *Gas Turbine Combustion*, Hemisphere, New York, 1983.

[10]Huang, R. F., and Lee, H. W., "Turbulence Effect on Frequency Characteristics of Unsteady Motions in Wake of Wing," *AIAA Journal*, Vol. 38, No. 1, 2000, pp. 87–94.

[11]Fiedler, H. E., "Control of Free Turbulent Shear Flows," *Flow Control—Fundamentals and Practices*, edited by M. Gad-el-Hak, A. Pollard, and J.-P. Bonnet, Springer-Verlag, Berlin, 1998, pp. 335–429.

[12]Hyman, H., "Suction Amplifier," U.S. Patent 3001539, Sept. 1961.
[13]Warren, R. W., "Negative Feedback Oscillator," U.S. Patent 3158166, Nov. 1964.
[14]Newman, B. G., "The Deflection of Plane Jets by Adjacent Boundaries—Coanda Effect," *Boundary Layer and Flow Control—Its Principles and Application*, Vol. 1, edited by G. V. Lachmann, Pergamon, New York, 1961, pp. 232–264.
[15]Tippetts, J. R., Ng, H. K., and Royle, J. K., "An Oscillating Bi-Stable Fluid Amplifier for Use as a Flowmeter," *Journal of Fluid Control*, Vol. 5, 1973, pp. 28–42.
[16]Yamasaki, H., and Honda, S., "A Unified Approach to Hydrodynamic Oscillator Type Flowmeters," *Journal of Fluid Control*, Vol. 13, 1981, pp. 1–17.
[17]Wang, H., Beck, S. B. M., Priestman, G. H., and Boucher, R. F., "A Remote Measuring Flow Meter for Petroleum and Other Industrial Applications," *Measurement Science and Technology*, Vol. 9, No. 5, 1998, pp. 779–789.
[18]Simoes, E. W., Furlan, R., and Pereira, M. T., "Numerical Analysis of a Microfluidic Oscillator Flowmeter Operating with Gases or Liquids, *Nanotech*, Vol. 1, No. 1, 2002, pp. 36–39.
[19]Yamamoto, K., Hiroki, F., and Hyodo, K., "Self-Sustained Oscillation Phenomena of Fluidic Flowmeters," *Journal of the Visualization*, Vol. 1, No. 4, 1999, pp. 387–396.
[20]Huang, B., "The Switch Fluidic Oscillator for Fluid Metering," *Proceedings of the Sixth International Conference on Flow Measurement*, Korea Research Inst. of Standards and Science, Taejon, Republic of Korea, 1993, pp. 416–423.
[21]Drazin, P. G., *Nonlinear Systems*, Cambridge Univ. Press, New York, 1992, pp. 214–229.
[22]Lalanne, L., Le Guer, Y., and Creff, R., "Dynamics of a Bifurcating Flow Within an Open Heated Cavity," *International Journal of Thermal Sciences*, Vol. 40, No. 1, 2001, pp. 1–10.
[23]Uzol, O., and Camci, C., "Experimental and Computational Visualization and Frequency Measurements of the Jet Oscillation Inside a Fluidic Oscillator," *Journal of the Visualization*, Vol. 4, No. 8, 2002, pp. 88–96.
[24]Camci, C., and Herr, F., "Forced Convection Heat Transfer Using a Self-Oscillating Impinging Planar Jet," *Journal of Heat Transfer*, Vol. 120, No. 4, 2002, pp. 770–782.
[25]Bejan, A., *Convective Heat Transfer*, Wiley, New York, 1984, pp. 110–114.
[26]Muller, T. J., "Flow Visualization by Direct Injection," *Fluid Mechanics Measurements*, 2nd ed., edited by R. J. Goldstein, Taylor and Francis, London, 1996, pp. 367–450.
[27]Flagan, R. C., and Seinfeld, J. H., *Fundamentals of Air Pollution Engineering*, Prentice–Hall, Englewood Cliffs, NJ, 1988, pp. 295–307.
[28]Glass, M., and Kennedy, I. M., "An Improved Seeding Method for High Temperature Laser-Doppler Velocimetry," *Combustion and Flame*, Vol. 29, June 1977, pp. 333–335.
[29]Mei, R., "Velocity Fidelity of Flow Tracer Particles," *Experiments in Fluids*, Vol. 22, No. 1, 1996, pp. 1–13.
[30]Hunt, J. C. R., Abell, C. J., Peterka, J. A., and Woo, H., "Kinematic Studies of the Flows Around Free or Surface-Mounted Obstacles; Applying Topology to Flow Visualization," *Journal of Fluid Mechanics*, Vol. 86, May 1978, pp. 179–200.

K. Fujii
Associate Editor